
Article:
Torelli, G. orcid.org/0000-0002-0607-695X, Gillie, M., Mandal, P. et al. (2 more authors) (2020) A moisture-dependent thermomechanical constitutive model for concrete subjected to transient high temperatures. Engineering Structures, 210. 110170. ISSN 0141-0296

https://doi.org/10.1016/j.engstruct.2020.110170

A moisture-dependent thermomechanical constitutive model for concrete subjected to transient high temperatures

Citation:
Torelli, G., Gillie, M., Mandal, P., Tran, V.-X., & Draup, J. (2020). A moisture-dependent thermomechanical constitutive model for concrete subjected to transient high temperatures. *Engineering Structures.*

Version:
Accepted for publication

A moisture-dependent thermomechanical constitutive model for concrete subjected to transient high temperatures

Giacomo Torelli[1*], Martin Gillie[2], Partha Mandal[3], Jefri Draup[4], Van-Xuan Tran[4]

[1] Department of Civil and Structural Engineering, University of Sheffield, Sheffield, S1 3JD, UK

[2] New Model in Technology & Engineering (NMiTE), Hereford, HR1 2HX, UK

[3]School of Mechanical, Aerospace and Civil Engineering, The University of Manchester, Manchester M13 9PL, UK

[4] EDF Energy, R&D UK Centre, 40 Grosvenor Place, London SW1X 7EN, UK

*Corresponding author, E-mail: g.torelli@sheffield.ac.uk Tel: +44 (0) 114 222 5796

Abstract

This paper presents a constitutive model for concrete able to capture the effects of the moisture content of the material on its mechanical behaviour under compressive loads and high transient temperatures. The model is the first to account for the experimentally demonstrated effect of moisture content on the two components of thermal strain, Load Induced Thermal Strain (LITS) and Free Thermal Strain (FTS). Both LITS and FTS are formulated as functions of the water content of the material at the beginning of the thermal transient. First, the theoretical formulation and numerical implementation of the model are presented. Then, the model is verified and validated against published transient tests on concrete specimens having different initial moisture contents. Finally, it is employed to assess a nuclear pressure vessel subjected to fault conditions. The results show that the model allows the moisture dependent behaviour of concrete heated under mechanical load to be accurately captured. Furthermore, it is shown the introduction of moisture-dependent thermal strain components is crucial to capture the behaviour of nuclear pressure vessels subjected to fault conditions. If the moisture-dependency of thermal strain of concrete is not considered, non-conservative results may be obtained.

Nomenclature

List of symbols

a, b	Polynomial coefficients
A_D	Pre-exponential diffusivity coefficient
B	Increment in LITS corresponding to a unit increment in temperature, normalized with respect to the load level σ/σ_{u0}, for temperatures higher than T_{crit}.
B_D	Exponential diffusivity coefficient
$B_{TDC}(\bar{C})$	Transient drying creep scaling function
C	Water content of the material
C_m	Triaxiality index for multiaxial load-induced thermal strain models
$\bar{C}$	Water content of the material prior to heating
D	Coefficient of diffusivity
E	Young's modulus of elasticity of material
$\bar{\bar{I}}$	Identity matrix
k_{tr}	Transient strain coefficient
Q_D	Drying activation energy
R	Universal gas constant ($R \approx 8.314$ J K^{-1} mol^{-1})
T	Temperature
$T_{D,0}$	Drying reference temperature
T_{dr}	Drying temperature
T_{max}	Maximum temperature ever reached by the material
T_{peak}	Temperature at which the maximum transient swelling expansion is expected to occur
α_1	Coefficient of thermal expansion in moisture-dependent models
α_2	Coefficient of transient shrinkage contraction
α_3	Coefficient of transient swelling expansion
α_D	Thermal diffusivity defined as the thermal conductivity divided by density and specific heat capacity at constant pressure
β_1	Uniaxial pure load-induced thermal strain derivative function
β_2	Transient drying creep derivative function
δ_{ij}	Kronecker symbol
γ	Triaxiality scaling factor for multiaxial load-induced thermal strain models
ε	Strain
$\varepsilon_{b\,cr}$	Basic creep strain
ε_{ela}	Elastic strain
ε_{fts}	Free thermal strain
ε_{lits}	Load-induced thermal strain
ε_{pfts}	Pure free thermal strain
ε_{plits}	Pure load-induced thermal strain
ε_{tsh}	Transient shrinkage strain
ε_{tdc}	Transient drying creep
$\varepsilon_{tsh,max}(\bar{C})$	Maximum transient shrinkage function
ε_{tsh}	Transient shrinkage
$\varepsilon_{tsw,\max}(\bar{C})$	Maximum transient swelling function
ε_{tsw}	Transient swelling

ε_{ttc}	Transient thermal creep strain
$\bar{\bar{\varepsilon}}_{ela}$	Elastic strain tensor
$\bar{\bar{\varepsilon}}_{fts}$	Free thermal strain tensor
$\bar{\bar{\varepsilon}}_{lits}$	Load-induced thermal strain tensor
$\bar{\bar{\varepsilon}}_{pfts}$	Pure free thermal strain tensor
$\bar{\bar{\varepsilon}}_{plits}$	Pure load-induced thermal strain tensor
$\bar{\bar{\varepsilon}}_{tdc}$	Transient drying creep tensor
$\bar{\bar{\varepsilon}}_{tot}$	Total strain tensor
$\bar{\bar{\varepsilon}}_{tsh}$	Transient shrinkage tensor
$\bar{\bar{\varepsilon}}_{tsw}$	Transient swelling tensor
η	Confinement coefficient for multiaxial load-induced thermal strain models
ν	Poisson's ratio
ν_{lits}	Load-induced thermal strain Poisson's ratio
σ	Stress
σ_{u0}	Compressive strength
$\bar{\bar{\sigma}}$	Stress tensor
$\bar{\bar{\sigma}}^{-}_{fin}$	Negative projection of the stress tensor at the end and of a generic time step
$\bar{\bar{\sigma}}^{-}_{ini}$	Negative projection of the stress tensor at the beginning and of a generic time step
$\bar{\bar{\sigma}}^{-}_{m}$	Mean value of the negative projection of the stress tensor at the beginning and at the end of a generic time step
$\underline{0}$	Null matrix of order 3×3

List of acronyms

FTS	Free Thermal Strain
LITS	Load-Induced Thermal Strain
PFTS	Pure Free Thermal Strain
PLITS	Pure Load-Induced Thermal Strain
TC	Transient Creep
TDC	Transient Drying Creep
TSH	Transient Shrinkage
TSW	Transient Swelling
TTC	Transient Thermal Creep

Keywords

Concrete; Temperature; Fire; Load-induced thermal strain; Transient thermal creep; Thermal strain; Stress confinement; Modelling; Moisture.

1 Introduction

If concrete is heated while simultaneously subjected to compressive mechanical loads, the thermal strain that develops depends on the stress level, as well on the temperature. For this reason, the thermal strain of concrete is commonly modelled as composed of two main parts: a load independent component, usually referred to as Free Thermal Strain (FTS), and a load dependent component, commonly known as Load-Induced Thermal Strain (LITS) [1–3]. The FTS is defined as the strain measured in stress free specimens subjected to thermal loads and it is usually an expansive strain component. It is the overall effect of the thermal expansions of aggregates and cement paste and the drying-induced shrinkage of the cement paste. On the other hand, LITS is defined as the additional contractive thermal strain component that develops in concrete when subjected to compressive stress. Such a strain component is experimentally obtained indirectly as the difference between the thermal strains measured in loaded and unloaded specimens subjected to the same thermal load. LITS is due to several stress-dependent mechanisms which develop on heating, such as thermomechanical strains related to chemical and physical reactions occurring in the cement paste, micro cracking effects, and micro diffusion of free water [1–3].

Catastrophic events such as the nuclear accident of Fukushima [4] and the Mont Blanc Tunnel fire [5] clearly demonstrated the necessity of accurate and reliable tools for the assessment of massive concrete structures under accidental heating. These accidents highlighted the potential advantages of material models able to capture the behaviour of concrete subjected to extreme thermomechanical loads so that the response of concrete structures to heating can be accurately assessed for the safety and security of society. This work aims to improve the existing techniques for modelling the behaviour of concrete subjected to combined transient thermal and compressive mechanical loads, with focus on the effects of the material moisture conditions on thermomechanical behaviour.

The two components of concrete thermal strain, FTS and LITS, are commonly modelled as independent of the moisture content of the material. FTS is usually seen as a solely temperature dependent strain component, while LITS is commonly modelled as a function of temperature and stress. However, experimental evidence

shows that, for unsealed concrete specimens subjected to thermal loads, both LITS and FTS significantly depend on the moisture condition of the material at the beginning of the thermal transient [6–9]. At ambient temperatures concrete drying is generally a long-term process that leads to the development of significant moisture gradients though the cross sections of concrete members. This suggests that, in the case of structures subjected to accidental transient high temperatures, concrete will exhibit a markedly non-homogenous and age-dependent behaviour, and hence for accurate predictions of structural behaviour, a material model that accounts for moisture effects is required.

In light of this, an original approach for assessing the moisture-dependent behaviour of heated concrete structures is presented here. It allows the dependency of the concrete thermal strains on the moisture condition of the material to be captured and, therefore, the effects of pre-accident drying and related moisture gradients on the mechanical behaviour of structures subjected to accidental thermal loads to be understood. The approach uses formulations of LITS and FTS material models which depend on the moisture content field in the material at the beginning of heating. Specifically, both LITS and FTS are split into their moisture-dependent and independent components, representing the macroscopic effects of the driving micro-mechanisms. The moisture concentration field at the beginning of the heating phase is obtained through a sequentially coupled thermal-hygral analysis. By describing LITS and FTS as a function of the moisture content field at the beginning of heating, no attempt is made to explicitly model the complex and still poorly understood mechanisms underlying moisture migration and evaporation phenomena occurring during high temperatures thermal transients. This allows modelling the thermo-hygro-mechanical problem through a simplified scheme involving a reasonably low number of parameters. The proposed moisture-dependent model allows assessing the effects of the age of a structure on its mechanical response under accidental cooling. In the case of design and predictive analyses, where the moisture content field at the beginning of heating is not known a priori, the model can be applied to assess the evolution of the thermo-mechanical performance of a structure with time. This can be done by performing multiple analyses where accidental heating is assumed to occur at different times. The model can also be used to perform forensic analyses. In this case, the moisture field at the beginning of heating can be assessed numerically as a function the age of the structure. Alternatively, when a concrete structure is monitored and data on the moisture distribution at the beginning of heating are available, a user-defined moisture field can be used. In the last section of this paper, the proposed LITS and FTS models are calibrated against experiments and adopted to assess the structural behaviour of a typical Prestressed Concrete Pressure Vessel (PCPV), such as those used in nuclear power stations, under accidental conditions.

2 Moisture dependency of concrete thermal strains

Over the years, many experimental studies have been performed to characterise the thermo-hygro-mechanical behaviour of unsealed concrete specimens subjected to transient thermal conditions [1,2,7–11]. These works demonstrate that both FTS measured in unloaded specimens and LITS in loaded concrete significantly depend on the curing regime for the specimens, i.e. these strains depend on initial moisture content and internal moisture movement on heating. Such a dependency is particularly significant for temperatures up to 200-300°C, where the evaporation of the free water takes place, but tends to disappear for higher temperatures [7,8]. Above such temperatures, the measured mass loss is mainly due to the drying-independent phenomenon of C-S-H dehydration [6,8]. Accordingly, for temperatures higher than 300°C, FTS and LITS in concrete specimens subjected to first-time heating at 0.2-1°C/min do not vary significantly with the initial water content of the material [2,6,8,9].

2.1 Moisture dependency of FTS

The FTS that develops in unloaded concrete specimens subjected to transient thermals is significantly sensitive to the moisture condition of the material for temperatures up to 200-300°C [6–8,12]. The hygral state of the material at the time of the temperature change not only affects the drying shrinkage of the cement paste on heating, but also influences its neat thermal expansion, i.e. the expansion occurring without overall loss of moisture [13–15]. This is commonly explained by considering the neat thermal expansion of the cement paste as made up of two contributions: a true kinetic and a swelling pressure expansion [12]. The true kinetic expansion corresponds to the actual thermal expansion of the cement gel. On the other hand, the swelling pressure expansion is an apparent material expansion due to a temperature-driven temporary increase in pressure in the water held by the gel pores, which causes the solid skeleton of the cement paste to expand. In the case of partially saturated concretes, an increase in temperature leads to a decrease in water cohesive forces, that is, a decrease in the capillary tension in the gel pores. This in turn increases the capillary action and results in a migration of water from capillary to gel pores and thus the appearance of a swelling pressure. This phenomenon cannot take place in completely dry concrete, because of the absence of free water in the capillary pores, nor in saturated concrete, because of the absence of capillary menisci in the gel pores. Such an explanation of the phenomenon is consistent with experimental results showing that, for ambient temperatures, the coefficient of thermal expansion of hardened cement pastes presents a maximum for a concrete relative humidity in the range 70 - 85% [13–15].

Given this background, an original modelling approach is proposed here that defines FTS ε_{fts} as the sum of a moisture independent component, referred to as Pure Free Thermal Strain (PFTS) $\bar{\bar{\varepsilon}}_{pfts}$, and two moisture dependent strains, called Transient Shrinkage (TSH) ε_{tsh} and Transient Swelling (TSW) ε_{tsw} respectively:

$$\varepsilon_{fts}(T, \bar{C}) = \varepsilon_{pfts}(T) + \varepsilon_{tsh}(T, \bar{C}) + \varepsilon_{tsw}(T, \bar{C}) \quad (2\text{-}1)$$

Where T is the temperature and $\bar{C}$ is a constant moisture field that correspond to the moisture distribution at the beginning of the transient thermal load. The PFTS component represents the thermal expansion induced by pure material expansion of aggregates and cement paste. The TSH component represents the thermal strain due to drying, i.e. the contraction caused by an overall loss of moisture. By contrast, TSW represents the temporary thermal expansion induced by micro diffusion of water from capillary pores to gel pores. Microdiffusion leads to a temporary increase in pressure in the water held by the gel pores, which causes the solid skeleton of the cement paste to expand. As it accounts for the effects of internal micro-diffusion, TSW depends on the initial moisture content of the materials but does not account for the effects of drying. Hence TSH and TWS reflect the tendency of the material to undergo two distinct micro mechanisms.

2.2 Moisture dependency of LITS

Hansen and Eriksson [11] found that LITS develops in concrete submerged under water, therefore demonstrating that part of it does not depend on drying. This drying-independent LITS component, here referred to as Pure Load-Induced Thermal Strain (PLITS) ε_{plits}, is due to i) an the increment in elastic strain $\varepsilon_{ela,T}$ induced by the rise in temperature, ii) a basic creep strain $\varepsilon_{b\,cr}$ developing during the heating phase iii) an additional thermomechanical strain occurring in the direction of the compressions, commonly referred to as Transient Thermal Creep (TTC) ε_{ttc} [1]. In a uniaxial context, the time derivative of PLITS developing in the direction of the applied stress can be decomposed as follows:

$$\dot{\varepsilon}_{plits} = \dot{\varepsilon}_{ela,T} + \dot{\varepsilon}_{b\,cr} + \dot{\varepsilon}_{ttc} \quad (2\text{-}2)$$

where σ represents the stress in the considered direction. TTC is generally the biggest component of LITS [2]. It is commonly considered to be driven by chemical and physical reactions taking place in the cement paste and, for temperatures higher than 300-400°C, by thermomechanical damage of concrete due to incompatibility between aggregate thermal expansion and cement paste contraction [1].

However, existing experimental research has shown that the LITS developing in unsealed heated concrete also depends on the moisture content of the material at the beginning of the heating phase [6–9]. This is due to the escape of moisture that occurs on heating under compressive loads, which causes the concurrent development of a drying creep strain [2]. Such a high temperature strain component is here defined as Transient Drying

Creep (TDC) ε_{tdc}, in order to distinguish it from the Drying Creep (DC), or "Picket effect" that develops for drying at ambient temperatures [16]. Accordingly, the LITS developing in unsealed concrete is here modelled as the sum of its drying-independent component, PLITS ε_{plits}, and its drying-dependent component, TDC ε_{tdc}:

$$\dot{\varepsilon}_{lits}(\sigma, T, \dot{T}, \bar{C}) = \dot{\varepsilon}_{plits}(\sigma, T, \dot{T}) + \dot{\varepsilon}_{tdc}(\sigma, T, \dot{T}, \bar{C}) \quad (2\text{-}3)$$

3 Moisture dependent thermal strain model

This section presents a novel modelling framework for capturing the dependency of concrete thermal strains on the moisture conditions in line with the experimental results discussed in Section 2.

3.1 Modelling strategy

The dependency of the thermal strains of concrete on the moisture condition of the material is captured here by expressing the moisture-dependent components of FTS and LITS as a function of the water content of the material at the beginning of the heating phase. In other words, this approach does not attempt to model the moisture changes that take place on heating explicitly, but assumes they develop for any material point as experimentally demonstrated for specimens subjected to unsealed conditions. This assumption allows modelling the thermo-hygro-mechanical behaviour of concrete in a relatively simple and intuitive manner and provides a tool for the assessment of the limit-behaviour of concrete structures whose permeability and hygral boundary conditions are uncertain. In fact, the validity of such an assumption depends on a number of factors which directly influence the moisture evacuation properties of the structure, but which can rarely been accurately known. These are, for example, the intrinsic permeability of the material, size of the considered concrete member, and presence of crack patterns or ducts facilitating the transport of mass. However, it is known in most cases, that the hygral boundary conditions of the material are between the limit cases of sealed conditions, where no moisture evacuation is allowed, and unsealed conditions, where the moisture evacuation is unobstructed. Thus, the proposed approach allows assessment of structural behaviour in the limiting case of unsealed conditions, and a comparison with the other limiting case of sealed conditions (which can be easily assessed by neglecting drying-dependent components of FTS and LITS).

According to the general strain decomposition presented in (2-1) the FTS that develops in initially moist concrete is here assumed to be the product of three main strain components, as shown in Figure 1. These are the moisture independent pure free thermal strain PFTS, corresponding to the thermal expansion of dry

concrete in Figure 1; the drying induced transient shrinkage TSH contraction; and the temporary swelling effect TSW.

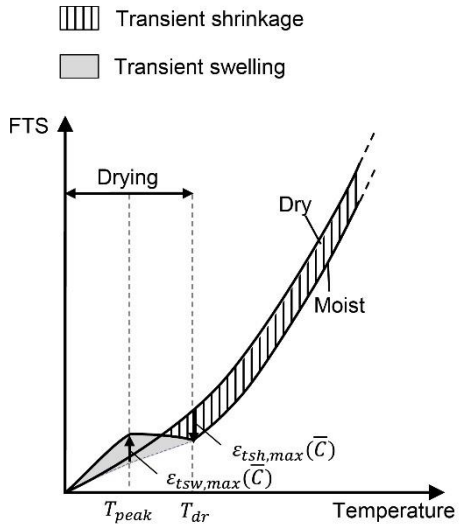

Figure 1 FTS developing in dry and moist concrete. Schematic representation of the transient shrinkage contraction (in red) and transient swelling effect (in blue) occurring for moist concrete.

In a similar manner, LITS is modelled as the product of the two strain components presented in (2-3). Such components, schematized in Figure 2, are the drying-independent pure load-induced thermal strain PLITS, corresponding to the thermal strain developing in dry concrete, and the transient drying creep strain TDC driven by concrete drying.

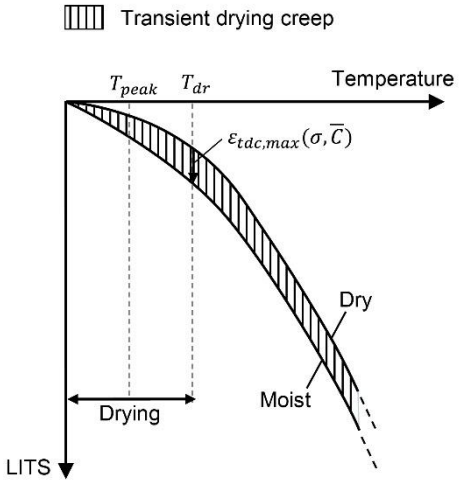

Figure 2 LITS developing in dry and moist concrete. Schematic representation of the transient drying creep contraction (in red) occurring for moist concrete.

The newly formulated uniaxial moisture-dependent LITS and FTS models and their 3D implementations are presented in detail in the following sections.

3.2 Moisture-dependent FTS model

According to the FTS decomposition presented in (2-1), the time derivative of the FTS $\dot{\varepsilon}_{fts}$ is:

$$\dot{\varepsilon}_{fts}(T,\dot{T},\bar{C}) = \dot{\varepsilon}_{pfts}(T,\dot{T}) + \dot{\varepsilon}_{tsh}(T,\dot{T},\bar{C}) + \dot{\varepsilon}_{tsw}(T,\dot{T},\bar{C}) \tag{3-1}$$

where $\dot{\varepsilon}_{pfts}(T,\dot{T})$, $\dot{\varepsilon}_{tsh}(T,\dot{T},\bar{C})$ and $\dot{\varepsilon}_{tsw}(T,\dot{T},\bar{C})$ are the time derivatives of the three components of FTS, namely PFTS, TSH and TSW. Such time derivatives have been defined for the three strain components PFTS, TSH and TSW to develop as schematized in Figure 1 for increasing temperatures. These profiles have been defined with a view of describing the experimentally observed macroscopic thermomechanical response of the material while involving a relatively small number of parameters.

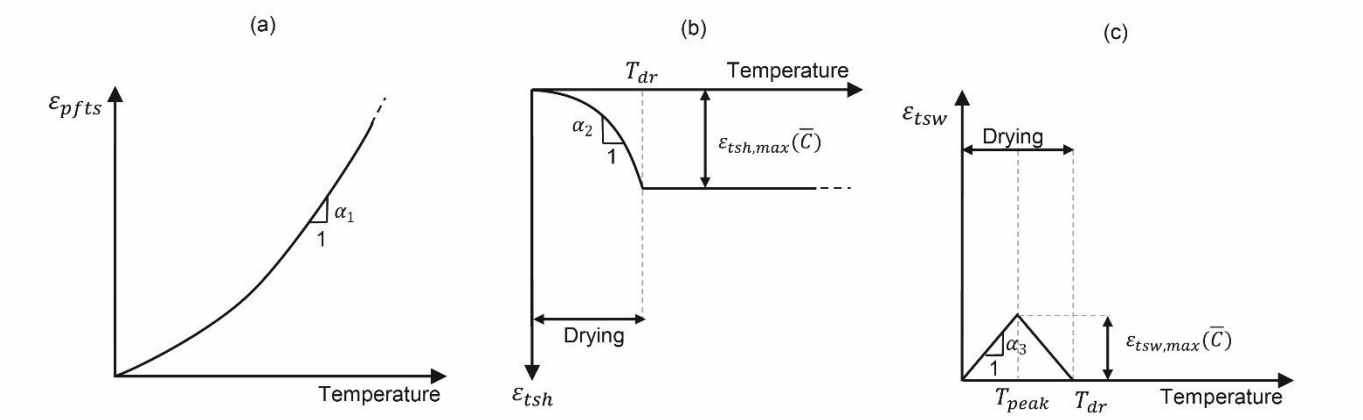

Figure 3 Temperature development of the three components of FTS: the moisture independent PFTS ε_{pfts} and the moisture dependent strain components TSH ε_{tsh} and TSW ε_{tsw}

Following the classic approach for modelling FTS [1], the moisture independent PFTS is here modelled as a function of the temperature only:

$$\dot{\varepsilon}_{pfts} = \alpha_1(T)\dot{T} \tag{3-2}$$

where α_1 is the coefficient of free thermal expansion, expressed as polynomial function of the temperature:

$$\alpha_1(T) = a_0 + a_1T + a_2T^2 + a_3T^3 + a_4T^4 + a_5T^5 \tag{3-3}$$

where the polynomial coefficients a_0, a_1, a_2, a_3, a_4 and a_5 are chosen to obtain the desired PFTS evolution with the temperature.

The moisture dependent TSH is defined as dependent on temperature and initial moisture condition:

$$\dot{\varepsilon}_{tsh} = \alpha_2(T, \bar{C})\dot{T} \tag{3-4}$$

where $\alpha_2(T, \bar{C})$ is the coefficient of TSH contraction, analogous to the coefficient of thermal expansion α_1, which describes the drying-induced shrinkage per unit increase in temperature. The coefficient is formulated so that TSH is a parabolic function of temperature, having zero initial slope (Figure 3). Imposing a zero initial slope allows the experimentally observed nonlinear development of drying shrinkage strains to be capture through a single parameter. In addition, TSH is imposed so as not to develop for temperatures higher than the drying temperature T_{dr}. This formulation allows the nonlinear development of TSH with temperature to be described with only one material parameter, $\varepsilon_{tsh,max}(\bar{C})$:

$$\alpha_2 = \begin{cases} 2\,\varepsilon_{tsh,max}(\bar{C})\dfrac{(T-20)}{(T_{dr}-20)^2} & for\ T < T_{dr} \\ 0 & for\ T \geq T_{dr} \end{cases} \tag{3-5}$$

where $\varepsilon_{tsh,max}(\bar{C})$ represents the maximum shrinkage strain, reached at the end of the drying phase (see Figure 3). This parameter is expressed as a function of the initial content of water $\bar{C}$ of the material, which can be defined by the user in a way that it equals zero for dry material, i.e. .e. for $\bar{C}$ = 0 l/m^3, and assumes growing negative values for growing initial water content.

Similarly, the moisture dependent TSW is modelled as dependent on temperature and initial moisture content:

$$\dot{\varepsilon}_{tsw} = \alpha_3(T, \bar{C})\dot{T} \tag{3-6}$$

where $\alpha_3(T, \bar{C})$ is the coefficient of TSW expansion, analogous to the coefficients α_1 and α_2 presented above. This coefficient describes the expansion due to the internal micro diffusion of water from capillary to gel pores for temperatures lower than a threshold temperature T_{peak}, as well as the contraction induced by the drying of gel pores water for higher temperatures. As schematized in Figure 3, $\alpha_3(T, \bar{C})$ is defined so that the TSW strain increases linearly with temperature for temperatures lower than a threshold temperature T_{peak} and decreases linearly to zero from T_{peak} to the drying temperature T_{dr}:

$$\alpha_3 = \begin{cases} \dfrac{\Delta\varepsilon_{tsw,max}(\bar{C})}{T_{peak} - 20°C} & for\ T < T_{peak} \\ -\dfrac{\Delta\varepsilon_{tsw,max}(\bar{C})}{T_{dr} - T_{peak}} & for\ T_{peak} \le T < T_{dr} \\ 0 & for\ T \ge T_{dr} \end{cases} \quad (3\text{-}7)$$

where $\Delta\varepsilon_{tsw,max}(\bar{C})$ and T_{peak} are two material parameters representing the maximum transient swelling expansion and the temperature at which this maximum is expected to occur respectively. A linear decrease of the transient swelling from $\Delta\varepsilon_{tsw,max}(\bar{C})$ at T_{peak} to zero at the drying temperature T_{dr} allows TSW to be defined as a temporary swelling effect that can be fully recovered to sufficiently high temperatures. The region $T < T_{peak}$ represents the temperature range in which, as discussed in Section 2.1, the rise in temperature determines a decrease in capillary tension. This induces a micro diffusion of water from capillary to gel pores which results in a material expansion. By contrast, the region $T_{peak} \le T < T_{dr}$ is the temperature range in which the gel pores dry due to the high level of energy provided to the material. This results in a material contraction that for $T = T_{dr}$ nullifies the micro diffusion expansion developing in the temperature range $20°C < T < T_{peak}$. For temperatures higher than the drying temperature T_{dr}, i.e. for material completely dried, the TSW increment has been imposed to be null.

The sensitivity of the TSW effect to the initial moisture condition of the material is captured by defining the maximum transient swelling expansion $\Delta\varepsilon_{tsw,max}(\bar{C})$ as a function of the initial water content.
This function is defined so that $\Delta\varepsilon_{tsw,max}(\bar{C})$ is null for completely dry and saturated material and presents a maximum for intermediate conditions. This is because, as discussed in Section 2.1, the micro diffusion of water can neither take place in completely dried material, due to the absence of water, nor in saturated concrete, due to the absence of capillary menisci.

3.3 Moisture-dependent LITS model

According to the LITS decomposition presented in (2-3), the time derivative of LITS $\dot{\varepsilon}_{lits}$ is:

$$\dot{\varepsilon}_{lits}(\sigma, T, \dot{T}, \bar{C}) = \dot{\varepsilon}_{plits}(\sigma, T, \dot{T}) + \dot{\varepsilon}_{tdc}(\sigma, T, \dot{T}, \bar{C}) \quad (3\text{-}8)$$

where $\dot{\varepsilon}_{plits}(\sigma, T, \dot{T})$ and $\dot{\varepsilon}_{tdc}(\sigma, T, \dot{T}, \bar{C})$ are the time derivatives of the two components of LITS, that is PLITS and TDC, respectively. The time derivatives of PLITS and TDC have been defined for PLITS and TDC to develop as schematized Figure 4 for growing temperatures.

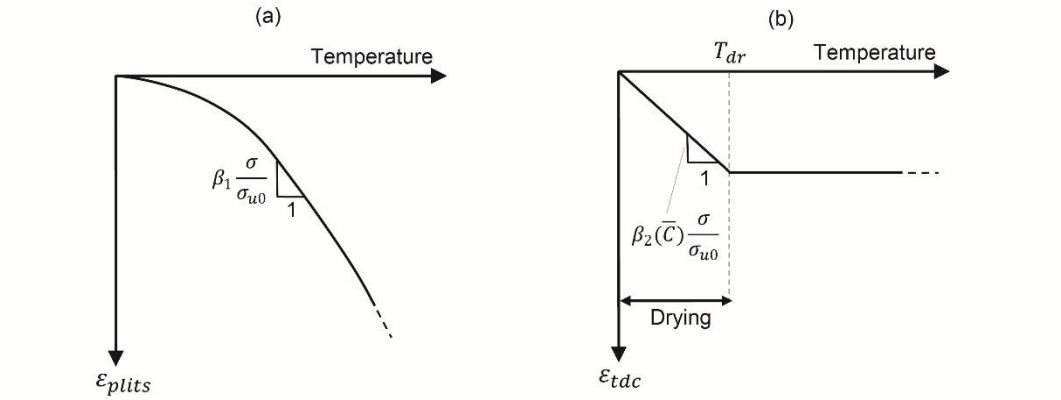

Figure 4 Temperature development of the two components of LITS: the moisture independent PLITS ε_{plits} and the moisture dependent strain TDC ε_{tdc}

The moisture-independent PLITS strain was modelled as only temperature and stress dependent, as previously done by the authors in [17]:

$$\dot{\varepsilon}_{plits} = \beta_1(T) \frac{\sigma}{\sigma_{u0}} \dot{T} \tag{3-9}$$

where σ is the stress in the considered direction, σ_{u0} the compressive strength of the material and $\beta_1(T)$ the LITS function, which is a generic function of temperature aimed at fitting the uniaxial temperature-LITS curve, here defined as a fourth-order polynomial of the temperature:

$$\beta_1(T) = b_0 + b_1 T + b_2 T^2 + b_3 T^3 + b_4 T^4 \tag{3-10}$$

where the polynomial coefficients b_0, b_1, b_2, b_3 and b_4 are material parameters chosen to fit the uniaxial LITS curve in the loaded direction

The moisture dependent TDC was defined as dependent on temperature, stress and initial moisture condition:

$$\dot{\varepsilon}_{tdc} = \beta_2(T, \bar{C}) \frac{\sigma}{\sigma_{u0}} \dot{T} \tag{3-11}$$

where $\beta_2(T, \bar{C})$ is the TDC derivative function which represents the increment in TDC per unit increment in temperature and stress level. Such a function has been defined in a way that TDC develops linearly with temperature while the material is simultaneously drying, and does not develop for temperatures higher than a threshold temperature T_{dr} representing the temperature at which the concrete drying process is complete (see Figure 4). The moisture dependency of TDC is included by defining the TDC derivative function as dependent on the initial moisture condition of the material:

$$\beta_2(T, \bar{C}) = \begin{cases} B_{TDC}(\bar{C}) & for\ T < T_{dr} \\ 0 & for\ T \geq T_{dr} \end{cases} \tag{3-12}$$

where $B_{TDC}(\bar{C})$ is a user defined function of the initial moisture condition $\bar{C}$ of the material, which allows scaling the development of TDC as a function of the initial water content of the material. $B_{TDC}(\bar{C})$ should be zero in the case of completely dry material, i.e. for $\bar{C} = 0$ l/m^3, and assume growing negative values for growing initial contents of water $\bar{C}$.

The modelling strategy adopted here allows all the required material parameters to be directly estimated from simple transient tests. However, it does not capture the effects of key microscale variables on the transient behaviour of the material. Indeed, the materials parameters defined here implicitly encapsulate the still not well understood effects of variables including pore size distribution, pore space connectivity and capillary pressure, on the macroscopic development of FTS and LIST. To identify the driving microscale variable and to explicitly model their effects on the behaviour of concrete subjected to transient thermal conditions, additional experimental and numerical work needs to be done.

An additional limitation of the proposed approach is that FTS and LITS are formulated as independent of the heating rate. Consequently, the effects of the heating rate on moisture transport properties, pore pressure and stress levels in the solid skeleton of the material are disregarded. Hence, the model should be calibrated against tests performed at heating rates comparable to those expected in situations of practical interests.

4 Constitutive relationship

The moisture-dependent thermal strain model presented in Sections 3.1, 3.2 and 3.3 has been implemented in a 3D thermoelastic material behaviour law. The constitutive relationship was implemented in the finite element solver *Code_Aster* [18] through the code generator *MFront* [19]. In this section, stress and strain states are expressed in 3D by second order tensors.

4.1 Implementation of the moisture dependent FTS and LITS models

In the light of experimental evidence, the uniaxial thermal strain model presented in Section 3.2 has been implemented in 3D by assuming that i) FTS develops isotopically and ii) LITS is proportional to both the stress tensor and the confinement of the stress state [10,20] and is irrecoverable on cooling or unloading [9,20–26]. Being driven by the temperature-induced moisture evacuation, the TSH has also been modelled as irrecoverable in terms of temperature. Similarly, the drying-related TSW contraction developing for $T_{peak} \leq$

$T < T_{dr}$ has been modelled as irrecoverable, based on the assumption that once the gel pores are emptied the moisture is evacuated, thus not re-enter the gel pore in the case of a subsequent decrease in temperature. By contrast, the TSW expansion that develops for $T < T_{peak}$ has been modelled as recoverable on cooling, based on the hypothesis that, in this temperature range, a change in temperature would only induce reversible internal moisture movements between gel and capillary pores.

. The qualitative development of the components of FTS and LITS in the case of heating-cooling cycles is illustrated in Figure 5 and Figure 6 respectively.

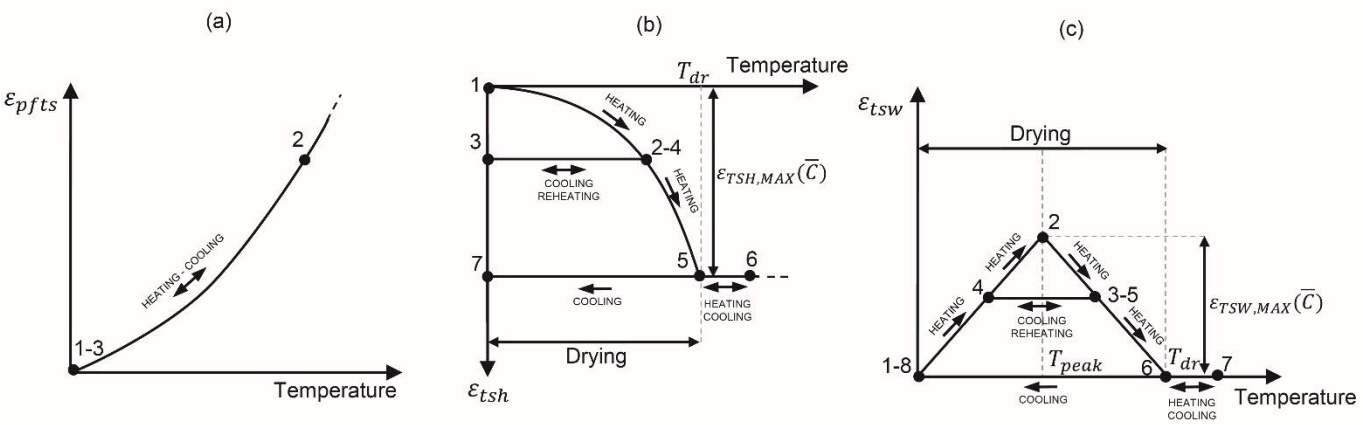

Figure 5 Qualitative development of the three components of the Free Thermal Strain (FTS) in the case of heating-cooling cycles: (a) PFTS, (b) TSH, (c) TSW.

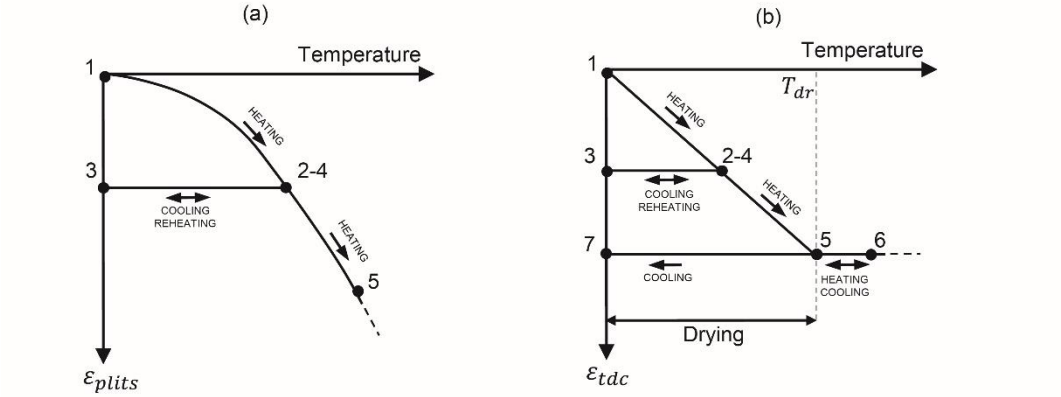

Figure 6 Qualitative development of the three components of the Free Thermal Strain (FTS) in the case of heating-cooling cycles: (a) PLITS, (b) TDC.

In line with previous work [17,27], the temperature history of the material is taken into account through an internal variable T_{max} which stores the maximum temperature ever reached by the material.

According Eq. (3-1), the increment in FTS tensor $\Delta\bar{\bar{\varepsilon}}_{fts}$ over a generic time step is defined as:

$$\Delta\bar{\bar{\varepsilon}}_{fts} = \Delta\bar{\bar{\varepsilon}}_{pfts} + \Delta\bar{\bar{\varepsilon}}_{tsh} + \Delta\bar{\bar{\varepsilon}}_{tsw} \tag{4-1}$$

where $\Delta\bar{\bar{\varepsilon}}_{pfts}$, $\Delta\bar{\bar{\varepsilon}}_{tsh}$ and $\Delta\bar{\bar{\varepsilon}}_{tsw}$ are the increment in PFTS, TSH and TSW respectively. The PFTS increment, representing the thermal expansion of the aggregates and the true kinetic expansion of the cement paste, is defined as perfectly recoverable in terms of temperature:

$$\Delta\bar{\bar{\varepsilon}}_{pfts} = \alpha_1(T)\, \Delta T\bar{\bar{I}} \tag{4-2}$$

The TSH has been imposed to develop only on first heating, i.e. not to develop on cooling or reheating. This choice was made by assuming concrete drying, which causes TSH, to be irrecoverable on cooling. In other words, it is assumed that when the pores are emptied the water is evacuated and does not re-enter the material on subsequent cooling. Accordingly, the TSH increment is defined as zero for temperatures lower than the maximum temperature ever reached T_{max}:

$$\Delta\bar{\bar{\varepsilon}}_{tsh} = \begin{cases} \underline{0} & for\ T \le T_{max} \\ \alpha_2(T, \bar{C})\, \Delta T\bar{\bar{I}} & for\ T = T_{max} \end{cases} \tag{4-3}$$

As discussed in Section 3.2, the TSW strain is assumed to be driven by internal micro diffusion of moisture from capillary to gel pores for temperatures lower than the threshold temperature T_{peak} and by drying of water contained in the gel pores for higher temperatures. With this in mind, the swelling strain induced by temperature rises for $T < T_{peak}$ is modelled as recoverable on cooling, while the drying-induced contraction developing for higher temperatures is imposed to be irrecoverable (see the qualitative development of TSW in the case of heating-cooling cycles reported in Figure 5). This was numerically obtained by implementing the increment $\Delta\bar{\bar{\varepsilon}}_{tsw}$ in TSW as:

$$\Delta\bar{\bar{\varepsilon}}_{tsw} = \begin{cases} \underline{0} & for\ T \le T_{max}\ \wedge\ \varepsilon_{tsw}(T_{\max}) \le \varepsilon_{tsw}(T) \\ \alpha_3(T, \bar{C})\, \Delta T\bar{\bar{I}} & otherwise \end{cases} \tag{4-4}$$

where $\varepsilon_{tsw}(T_{\max})$ and $\varepsilon_{tsw}(T)$ are the values assumed by the transient swelling function for the maximum temperature T_{max} reached by the material and the current temperature T respectively:

$$\varepsilon_{tsw}(T_{MAX}) = \begin{cases} \alpha_{3,1} T_{max} & T_{max} < T_{peak} \\ \alpha_{3,1} T_{peak} - \alpha_{3,2} T_{max} & T_{peak} \leq T_{max} < T_{dr} \\ 0 & T_{max} \geq T_{dr} \end{cases} \quad (4\text{-}5)$$

$$\varepsilon_{tsw}(T) = \begin{cases} \alpha_{3,1} T & T < T_{peak} \\ \alpha_{3,1} T_{peak} - \alpha_{3,2} T & T_{peak} \leq T < T_{dr} \\ 0 & T \geq T_{dr} \end{cases} \quad (4\text{-}6)$$

where:

$$\alpha_{3,1} = \frac{\Delta\varepsilon_{tsw,max}(\bar{C})}{T_{peak} - 20°C} \quad (4\text{-}7)$$

$$\alpha_{3,2} = \frac{\Delta\varepsilon_{tsw,max}(\bar{C})}{T_{dr} - T_{peak}} \quad (4\text{-}8)$$

Following the LITS decomposition reported in Eq. (3-8), the increment $\Delta\bar{\bar{\varepsilon}}_{lits}$ in LITS was defined as:

$$\Delta\bar{\bar{\varepsilon}}_{lits} = \Delta\bar{\bar{\varepsilon}}_{plits} + \Delta\bar{\bar{\varepsilon}}_{tdc} \quad (4\text{-}9)$$

where $\Delta\bar{\bar{\varepsilon}}_{plits}$ and $\Delta\bar{\bar{\varepsilon}}_{tdc}$ are the increment in PLITS and TDC respectively, representative of the macroscopic effect of chemical and physical reactions taking place in the cement paste (PLITS) and concrete drying under mechanical loading (TDC). Based on experimental evidence, both components have been modelled as irrecoverable on cooling by imposing a zero LITS increment for temperatures lower than the maximum temperature ever reached T_{MAX} [9,20–26]. The uniaxial LITS model described by Eq. (3-8), (3-9), (3-10), (3-11) and (3-12) has been extended to 3D through the confinement dependent approach presented by the authors in [17,27], which captures the dependency of LITS on stress confinement through a confinement coefficient η:

$$\begin{cases} \Delta\bar{\bar{\varepsilon}}_{lits} = \underline{0} & for\ T \leq T_{max} \\ \Delta\bar{\bar{\varepsilon}}_{lits} = \eta \left[\frac{\beta_1(T) + \beta_2(T, \bar{C})}{\sigma_{u0}}\right] \left((1 + \upsilon_{lits})\bar{\bar{\sigma}}_m^- - \upsilon_{lits} tr(\bar{\bar{\sigma}}_m^-)\bar{\bar{I}}\right) \Delta T & for\ T = T_{max} \end{cases} \quad (4\text{-}10)$$

where $\bar{\bar{\sigma}}_m^-$ is the mean value of the negative projection of the stress tensor over the considered time step, obtained as the mean of the negative projection of the stress tensor at the beginning of the time step $\bar{\bar{\sigma}}_{ini}^-$ and at the end of the time step $\bar{\bar{\sigma}}_{fin}^-$, υ_{lits} a material parameter defined as the negative ratio of transverse to axial LITS strain, analogous to the elastic Poisson's modulus υ, and η is the confinement coefficient defined as:

$$\eta = 1 + (C_m - 1)\gamma \quad (4\text{-}11)$$

where C_m in a triaxialily index automatically evaluated at each time step as a function of the negative projections of principal stresses σ_1^-, σ_2^- and σ_3^-:

$$C_m = \frac{|\sigma_1^- + \sigma_2^- + \sigma_3^-|}{\sqrt{(\sigma_1^-)^2 + (\sigma_2^-)^2 + (\sigma_3^-)^2}} \tag{4-12}$$

and γ is a user-defined triaxiality scaling factor.

4.2 General strain decomposition

The 3D model presented in section 4.1 has been implemented in a thermo-elastic material behaviour law. The increment $\Delta\bar{\bar{\varepsilon}}_{tot}$ in total strain is defined as:

$$\bar{\bar{\varepsilon}}_{tot} = \Delta\bar{\bar{\varepsilon}}_{ela} + \Delta\bar{\bar{\varepsilon}}_{fts} + \Delta\bar{\bar{\varepsilon}}_{lits} \tag{4-13}$$

where $\Delta\bar{\bar{\varepsilon}}_{fts}$ and $\Delta\bar{\bar{\varepsilon}}_{lits}$ are the increment in FTS and LITS defined in Section4.1 and $\Delta\bar{\bar{\varepsilon}}_{ela}$ is the increment in elastic strain:

$$\Delta\bar{\bar{\varepsilon}}_{ela} = \frac{1+\upsilon}{E}\Delta\bar{\bar{\sigma}} - \frac{\upsilon}{E}tr(\Delta\bar{\bar{\sigma}})\bar{\bar{I}} \tag{4-14}$$

where $\Delta\bar{\bar{\sigma}}$ is the stress tensor increment, E the Young's modulus and υ the Poisson's ratio. In the present model, the temperature-driven reduction in stiffness of the material is accounted for in $\Delta\bar{\bar{\varepsilon}}_{lits}$. Accordingly, E should be treated as the ambient temperature Young's modulus, i.e. it should be defined as temperature-independent to avoid considering the elastic contribution twice.

It is worth noting that the FTS and LITS models presented in section 4.1 could also be included in more comprehensive concrete constitutive models. Indeed, when applied to situations involving relatively high stress levels and thermal gradients, the general strain decompositions reported in equation (4-15) fails to capture ambient-temperature damage/microcracking and plastic strains. Similarly, the time-dependent concrete strains are disregarded. Ambient-temperature damage/microcracking, plastic and creep strain components could be included in the model, leading to the following strain decomposition:

$$\bar{\bar{\varepsilon}}_{tot} = \Delta\bar{\bar{\varepsilon}}_{ela} + \Delta\bar{\bar{\varepsilon}}_{d} + \Delta\bar{\bar{\varepsilon}}_{pl} + \Delta\bar{\bar{\varepsilon}}_{cr} + \Delta\bar{\bar{\varepsilon}}_{fts} + \Delta\bar{\bar{\varepsilon}}_{lits} \tag{4-15}$$

Where $\Delta\bar{\bar{\varepsilon}}_d$ is the strain component due to mechanical damage of the material, $\bar{\bar{\varepsilon}}_{pl}$ the plastic strain and $\Delta\bar{\bar{\varepsilon}}_{cr}$ the time-dependent isothermal creep strain. Examples of thermal strain models implemented in constitutive laws including damage and plasticity are reported in [28,29]. In the present work, implementing the newly developed moisture-dependent FTS and LITS components in a thermo-elastic material behaviour law was deemed to be appropriate. Indeed, this allowed for rigorous validation against tests performed at low stress levels and thermal gradients, hence not involving non-linear behaviour due to ambient-temperature mechanical damage, and to obtain an insightful indication of the effects of moisture on the thermomechanical behaviour of a concrete vessel subjected to fault conditions.

4.3 Numerical methods

The behaviour law has been implemented to solve static nonlinear mechanical analyses through a *Newton-Raphson* iterative method with tangent matrix prediction [30,31]. At a Gauss point level, the behaviour law is integrated through an implicit method based on a *Newton-Raphson* scheme and a jacobian matrix obtained by a second order finite difference [19].

4.4 Thermal and drying analysis methods

The mechanical behaviour law presented in the previous sections depends on the current temperature T, on the maximum temperature ever reached T_{max}, and on the water content $\bar{C}$ of the material prior to heating. Thus, the mechanical analysis is included in a sequentially coupled thermo-hygro-mechanical analysis scheme (see Figure 7).

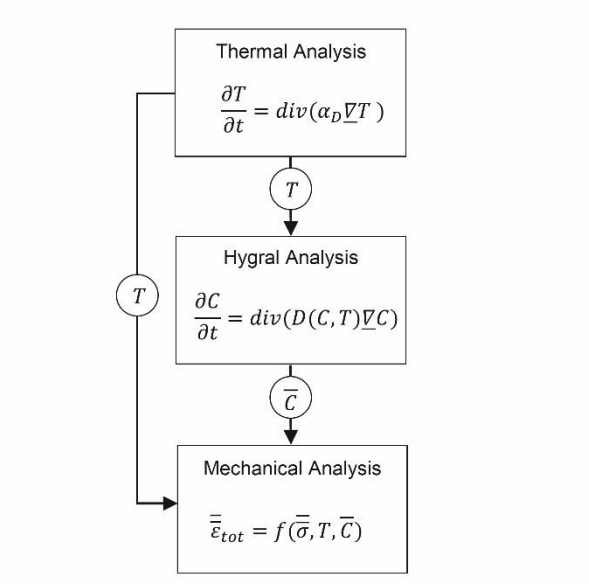

Figure 7 Thermo-hygro-mechanical analysis scheme.

First, the evolution of the temperature field is obtained through a nonlinear thermal analysis. The thermal model adopted here is represented by a diffusion equation obtained from the energy conservation:

$$\frac{\partial T}{\partial t} = div(\alpha_D \underline{\nabla} T) \tag{4-16}$$

where T is the temperature, t is the time and $\alpha_D(T)$ is the thermal diffusivity coefficient of the material, defined as the thermal conductivity $\lambda(T)$ divided by density ρ and specific heat capacity at constant pressure $c_p(T)$. Then, the hygral state of the material prior to accidental heating is calculated through a nonlinear hygral analysis which takes into account the effects of the temperature gradient obtained via the thermal analysis [32]. The hygral analysis is stopped at the beginning of the accidental heating phase to obtain the moisture field prior to heating, needed to inform the mechanical analyses. The drying of concrete is modelled by a diffusion law which takes into account the migration of both liquid and vapour phase within the material:

$$\frac{\partial C}{\partial t} = div(D(C,T)\underline{\nabla} C) \tag{4-17}$$

where C is the water content of the material, t is the time and D is the diffusivity, which is calculated as a function of C and T according the Granger's law [32]:

$$D(C,T) = A_D \exp(B_D C) \frac{T}{T_{D,0}} \exp\left[-\frac{Q_s}{R}\left(\frac{1}{T} - \frac{1}{T_{D,0}}\right)\right] \tag{4-18}$$

where R is the universal gas constant, Q_D the drying activation energy, $T_{D,0}$ the reference drying temperature, and A_D and B_D two material parameters governing the ambient temperature diffusivity, named the pre-exponential and the exponential diffusivity coefficient respectively.

Finally, the evolution of the temperature field obtained through the thermal analyses and the initial hygral state evaluated by the hygral analysis are used as input variables for the mechanical analysis. Note that, within this framework, the physical and chemical changes taking place in the microstructure of the material at high temperatures and the consequent full coupling between thermal, hygral and mechanical behaviour is not explicitly modelled. However, the main effects of these phenomena on the thermal properties of the material are implicitly considered by defining both the thermal conductivity $\lambda(T)$ and the specific heat capacity $c_p(T)$ as function of the temperature.

5 Verification and validation studies

5.1 Reference experiments

The mechanical model proposed in this paper is calibrated by taking as a reference the experimental results reported in [7], where the effect of the initial moisture content on the development of FTS and LITS was investigated systematically. These data have been deemed to be particularly meaningful because they were obtained through a statistical analysis of the results of 130 transient tests performed on specimens made of five different types of concrete mixes, based on limestone, basalt, gravel and lightweight aggregate respectively. Furthermore, the transient tests considered were performed at the relatively low heating rate of 0.2°C/min, which ensured the development of reasonably homogeneous temperature and drying fields throughout the specimens on heating and therefore correspondence in behaviour between specimens and ideal concrete material points.

The transient tests were performed on unsealed concrete cylinders, with dimension of 186 mm height and 62 mm diameter, having various initial moisture conditions. Specifically, initial water contents of 5.40%, 4.40% and 0% in terms of weight were studied. The water contents discussed above are expressed in terms of "moist" weight, i.e. they represent the experimentally determined ratio between the weight of water and the weight of moist concrete. For full details see Khoury et al. [7].

5.2 FE models and results

Given the axial symmetry of the problem, the size of the analyses has been minimized by modelling only one quarter of the cylindrical specimens using second-order hexahedral finite elements (see Figure 8). The three faces lying on the symmetry planes $x = 0$ m, $y = 0$ m and $z = 0$ m were prevented from translating in their normal directions. A uniformly distributed pressure σ was applied to the face lying at $z = 0.186$ m.

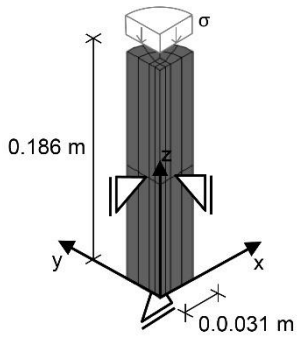

Figure 8 Mesh, boundary and loading conditions defined for modelling the uniaxial transient tests reported in [7]

First, a thermal analysis was performed to assess evolution of the temperature field on heating. A heating rate of 0.2°C/min, equal to the experimental one [10], was applied to the lateral surfaces of the specimen. According to the recommendations provided by the Eurocode 2, thermal conductivity λ and volumetric specific heat c_v were defined as temperature-dependent parameters [29]. The thermal conductivity curve λ(T) was defined as the average of the upper and lower limit functions provided by the Eurocode. The heat capacity curve $c_p(T)$ proposed by Eurocode 2 for an initial moisture content of 3% was adopted for all the analysed specimens. The choice of using the same $c_p(T)$ curve for specimens having different initial moisture contents was made in the light of a preliminary sensitivity study which showed that, for a relatively slow heating rate of 0.2°C/min, the effect of the initial moisture content on the thermal analysis is negligible. Specifically, it was found that the maximum relative difference between the temperatures predicted for dry and moist concrete at the core of the specimen was less than 0.04%.

Five different levels of initial water content were considered: the three moisture contents considered in the experiments, i.e. C=0 l/m^3, C=106 l/m^3 and C=130 l/m^3, and two intermediate values C=50 l/m^3 and C=118 l/m^3. In these verification studies the water content levels were imposed as uniform fields.

Then, the mechanical analyses were performed through the moisture-dependent constitutive relationship presented in Section 0. The evolution of the moisture dependent material parameters $\varepsilon_{tsh,max}(\bar{C})$, $\varepsilon_{tsw,max}(\bar{C})$ and $B(\bar{C})$ with the water content has been defined so as to fit the experimental data and is illustrated in Figure 9a, 9b and 9c. The values adopted for the other parameters are reported in Table 1. It

is worth noting that, in the present work, the FTS and LITS material parameters have been calibrated against transient tests performed on concrete mixes with a water/cement ratio in the range 0.3-0.32 and a 67% aggregate volumetric content [7]. Hence, the best way to accurately capture the behaviour of concrete mixes with different mix proportions is to re-calibrate the models via additional transient tests. However, when experimental data are unavailable or the concrete composition is unknown (e.g. in the design phase), it is reasonable to use the coefficient obtained here.

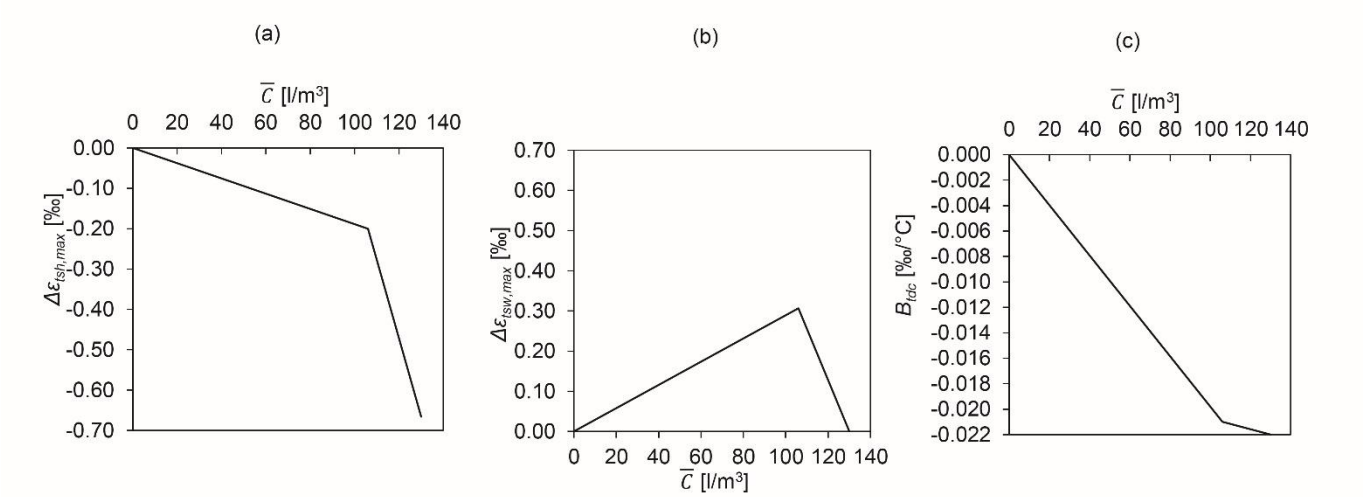

Figure 9 Moisture-dependent functions: a) Maximum expected transient shrinkage $\varepsilon_{tsh,max}$; b) Maximum expected transient swelling $\varepsilon_{tsw,max}$; c) TDC coefficient B_{tdc}.

Table 1: Moisture-independent material parameters

Material parameter	Value
E	47000 MPa
ν	0.25
ν_{LITS}	0.48
γ	2.68
b_0	-8.453367e-05 °C^{-1}
b_1	2.946952e-06 °C^{-1}
b_2	-3.264034e-08 °C^{-1}
b_3	1.434291e-10 °C^{-1}
b_4	-2.780193e-13 °C^{-1}
a_0	-2.29070e-06 °C^{-1}
a_1	2.84651e-07 °C^{-1}
a_2	-2.81933e-09 °C^{-1}
a_3	1.20736e-11 °C^{-1}
a_4	-2.33299e-14 °C^{-1}
a_5	1.68298e-17 °C^{-1}

Figure 10 and Figure 11 show a comparison between experimental and numerical FTS and LITS curves for the various levels of water content considered. The same results are also plotted in terms of moisture dependent components of FTS and LITS in Figure 12 and Figure 13. The match between experimental and numerical thermal strain curves demonstrates the capability of the approach to take the experimentally observed moisture dependency of the thermal strains into account.

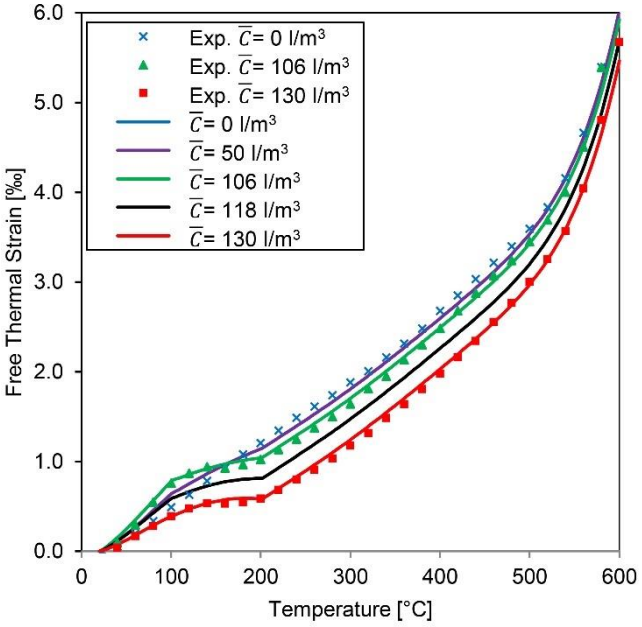

Figure 10 Experimental FTS curves [7] and numerical results.

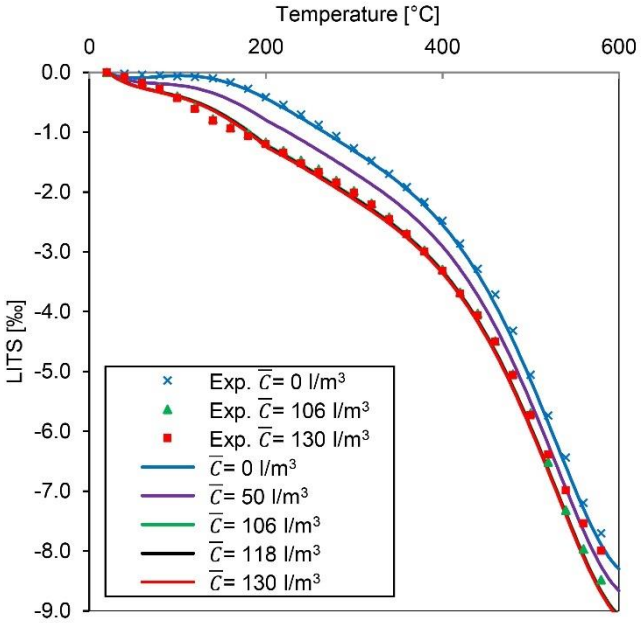

Figure 11 Experimental LITS curves [7] and numerical results. Load level 20%.

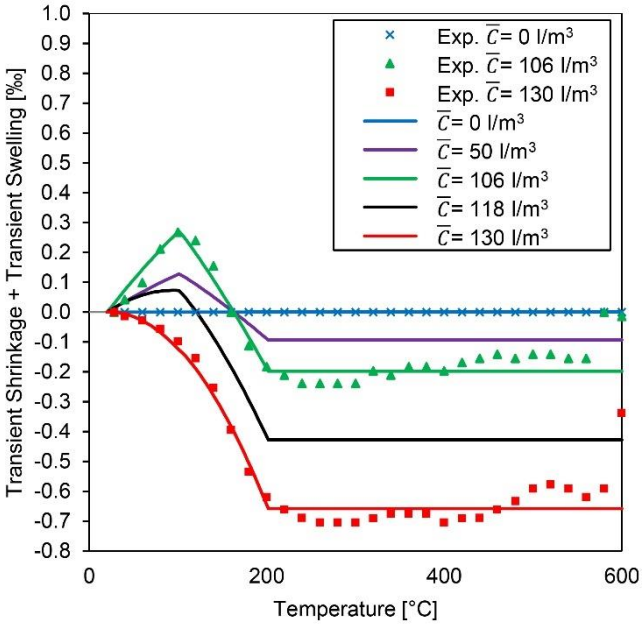

Figure 12 Moisture-dependent part of the FTS: TSH + TSW. Comparison between experimental [7] and numerical results.

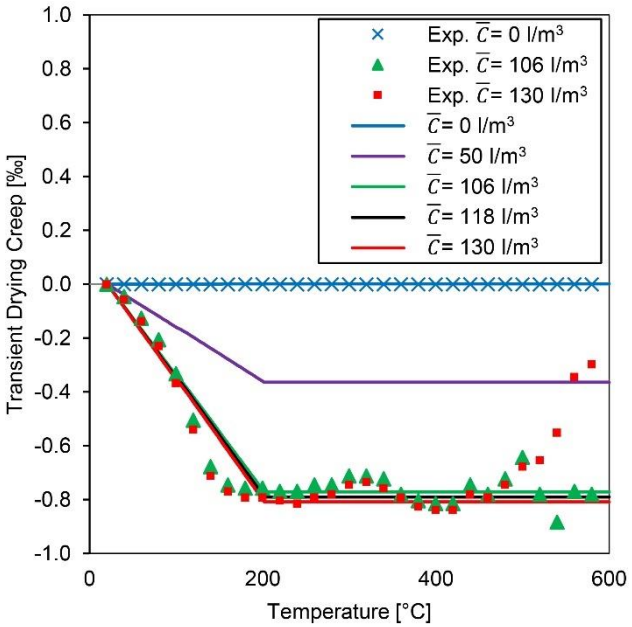

Figure 13 Moisture-dependent part of LITS: TDC. Comparison between experimental [7] and numerical results. Load level 20%.

6 Assessment of a PCPV subjected to fault conditions

The calibrated moisture-dependent model was next used to assess the effect of the moisture dependent thermal strain components on the structural behaviour of a nuclear PCPV subjected to accidental heating-cooling cycles. The PCPVs of Advanced Gas-cooled Reactors (AGRs) are nuclear containment structures designed to

hold the gas coolant, whose service temperature is about 500-600°C. For normal operating conditions, the temperature of the concrete is kept at about 50°C by a water cooling system. In this study, *short term* and *long term* temporary faults of the cooling pipes system are modelled by a applying heating-cooling cycles to the internal surface of the vessel. Specifically, the temperature of the internal surface of the vessel was imposed to stay constant at 600°C for 2 days (*short term* fault condition) and 14 days (*long term* fault condition).

The thermo-hygro-mechanical problem was solved by following the sequentially coupled thermo-hygro-mechanical analysis scheme discussed in section 4.3. As per Figure 7, a thermal analysis was first conducted to determine the evolution of the temperature field throughout the whole life of the structure, including accidental fault. Then, the moisture field prior to heating is calculated through a hygral analysis that considers the effects of the evolution of the temperature field obtained via the thermal analysis. The hygral analysis is stopped at the beginning of the heating phase to obtain the moisture field prior to heating, needed to inform the mechanical analyses. The mechanical analysis if finally performed by taking into account the evolution of the temperature field during the fault, obtained through thermal analysis, and the moisture field at the beginning of heating, calculated by hygral analysis.

6.1 FE model

A typical cylindrical PCPV having a 4.5-meters-thick lateral wall and pre-stressed by vertical and hoop tendons was considered (see Figure 14). The stress-strain state at mid-height of the wall was studied by modelling a representative parallelepiped-shaped portion of the vessel, therefore neglecting the effects of the relatively small curvature of the wall itself. As shown in Figure 14, the analysed representative volume extends through the whole thickness of the wall and has dimensions 0.5m x 0.5m x 4.5m. A similar modelling approach was adopted in [17]. A pre-stressing system composed of 8 layers of vertical and hoop tendons was considered.

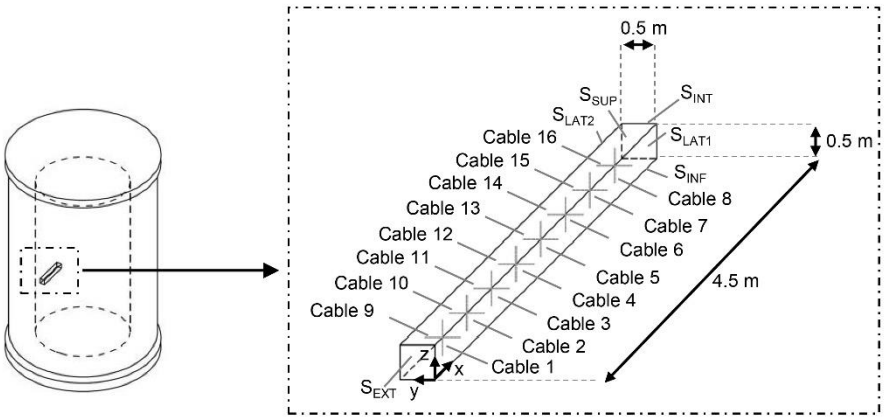

Figure 14 Typical PCPV geometry and studied representative portion. Adapted from [17].

The representative volume of concrete was meshed by hexahedral elements, while the steel tendons were modelled by bar elements perfectly bonded to the concrete volume. The constraining effect of base and top cap on the mechanical behaviour of the vessel at mid height of the wall was considered to be negligible [32]. With reference to Figure 14, the kinematic boundary conditions of the representative portion were defined so as to allow the volume to expand and contract along the direction *x*, *y* and *z*. This was done by preventing the faces S_{INT}, S_{LAT1} and S_{INF} from translating along their normal directions.

Following the approach schematized in Figure 7, the structural behaviour of the vessel was assessed through a sequentially coupled thermo-hygro-mechanical analysis. The thermo-hygral state of the vessel at the beginning of the fault condition was obtained by modelling the whole life of the structure. The following life phases were considered:

- Construction (8 years)
- Normal operation (30 years)
- Fault (2 days for *short term* fault; 14 days for *long term* fault).

During the whole life of the structure, an ambient temperature of 20°C was assigned to the external surface of the vessel. The temperature of the internal surface was assumed to be 20, 50 and 600°C during construction, normal operation and fault phases respectively. For the hygral analysis, the external surface of the vessel was considered to be open to the atmosphere during the whole life of the structure. This has been modelled by assigning a constant water concentration of 50 l/m^3 to the external surface of the wall. During the first 5 years of life of the structure, a water concentration of 50 l/m^3 was also assigned to the internal surface. However, it was assumed that after 5 years a gas proof steel liner is applied to the internal surface of the vessel, thereafter preventing the exchange of moisture with the environment. Accordingly, the mass flux though the internal surface of the wall is imposed to be null after the first 5 years. As for the verification studies, thermal conductivity λ and volumetric specific heat c_v of the material were defined according to the recommendations provided by the Eurocode 2 – see Section 5. The adopted drying material parameters are reported in Table 1.

Table 1 Drying analysis material parameters

Material parameter	Value
A	3.3 10^{-13} m^2/s
B	0.05
T_0	20 °C
Q_S/R	4000 °C

The tension of the tendons was set to be 920 kN at the beginning of the fault of the cooling system. The mechanical analyses were aimed at assessing the loss in prestress caused by *short* and a *long* term fault conditions, as well as the effect of each concrete and steel strain component on the structural response of the vessel. The thermo-hygro-mechanical material behaviour presented in Section 0 was applied to the concrete volume and the material parameters calibrated in Section 5 and given Table 1 were adopted. The steel of the tendons was modelled as an elastic material, having Young's modulus $E = 200000$ MPa, Poisson's modulus $v = 0.3$ and coefficient of thermal expansion $\alpha = 8 \times 10^{-6}$ °C^{-1}. The effect of the various concrete and steel strain components on the structural behaviour of the vessel under fault conditions was evaluated by activating them in various combinations, as schematised in Table 2. In addition, the effect of the initial water content on the behaviour of the structure was studied by adopting three different initial hygral fields: the one evaluated through the thermo-hygral analysis and two imposed homogeneous fields of $\bar{C}$=106 l/m^3 and $\bar{C}$=130 l/m^3, representative of the experimental "air died" and "moist" conditions analysed in [7] respectively (see Table 2).

Table 2 Active (×) and inactive (-) strain components and hygral fields considered for the various types of analyses performed.

Analysis type	Steel		Concrete						Hygral field
	ε_{el}	ε_{fts}	ε_{el}	ε_{pfts}	ε_{tsh}	ε_{tsw}	ε_{plits}	ε_{tdc}	
(a)	×	-	×	-	-	-	-	-	-
(b)	×	×	×	-	-	-	-	-	-
(c)	×	-	×	×	-	-	-	-	-
(d)	×	×	×	×	-	-	-	-	-
(e)	×	×	×	×	-	-	×	-	-
(f)	×	×	×	×	×	×	×	×	From hygral analysis
(g)	×	×	×	×	×	×	×	×	Imposed $\bar{C}$=106 l/m^3
(h)	×	×	×	×	×	×	×	×	Imposed $\bar{C}$=130 l/m^3

6.2 Results and discussion

As shown in Figure 15, after 30 years of operation the temperature field is steady and varies linearly from 20°C (external surface) to 50°C (internal surface) along the thickness of the wall. However, the massive structure of the PCPV allows it to absorb heat efficiently in the case of a temporary fault of the cooling pipes system: only a relatively thin layer of concrete next to the internal surface is affected by the temperature rise – see Figure 16 and Figure 17. Specifically, the thickness of interest layer ranges from approximately *1* m in the case of *short term* fault to about *2* m in the case of *long term* fault. After the fault is fixed and the internal surface of vessels returns to its service temperature of 20°C, the affected region of the wall cools down and approaches the temperature state prior to the heating in approximately one week in the case of *short term* fault and two weeks in the case of *long term* fault.

Because of the size of the structure the drying process is extremely slow and most of the material has not dried after 30 years of operation. Figure 18 shows that only two relatively thin layers of material next to the internal and external surfaces are subjected to drying during the first 5 years of construction. Then, the gas proof steel liner applied to the internal surface prevents the adjacent material to dry further. Consequently, only the external layer of material keeps drying for the rest of the vessel life, while a local moisture redistribution takes place in the region next the internal surface of the wall after the liner is applied. At the beginning of the fault

conditions, the material next to the internal surface of the vessel, i.e. the material which is affected the most by the accidental temperature transient, has a water content of about 120 l/m^3 (see Figure 18).

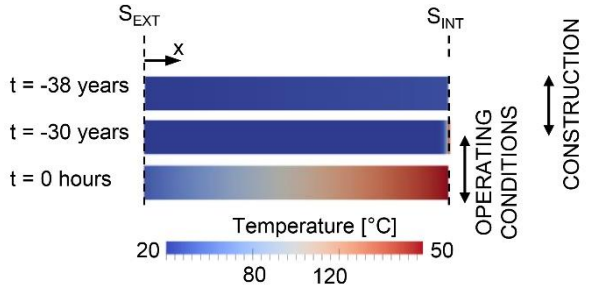

Figure 15 Evolution of the temperature field though the thickness of the PCPV lateral wall during the first 38 years of life of the structure: construction (8 years) + normal operation (30 years). $x(S_{EXT})$ = 0m, $x(S_{INT})$ = 4.5m.

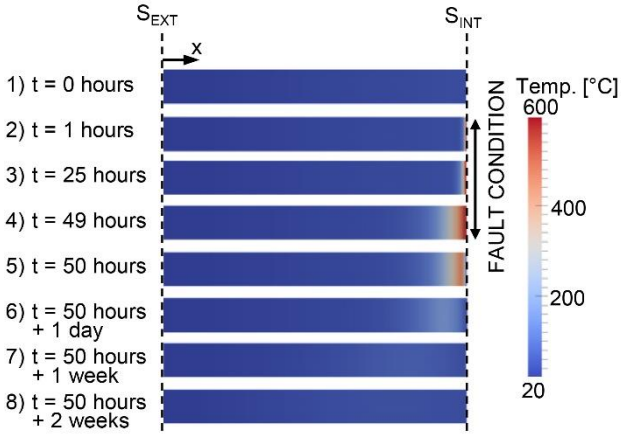

Figure 16 Evolution of the temperature field though the thickness of the PCPV lateral wall. *Short term* fault condition (2 days). $x(S_{EXT})$ = 0m, $x(S_{INT})$ = 4.5m.

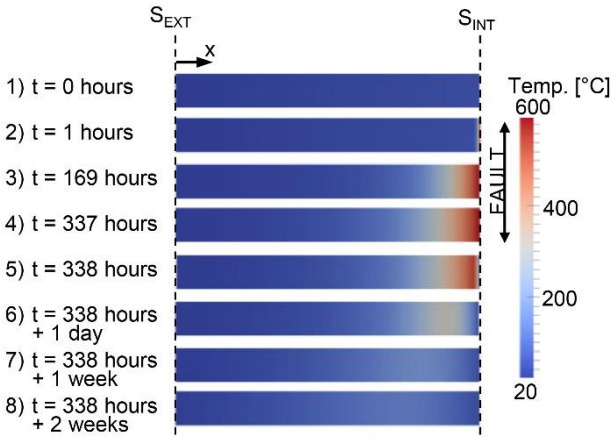

Figure 17 Evolution of the temperature field though the thickness of the PCPV lateral wall. *Long term* fault condition (14 days). $x(S_{EXT})$= 0m, $x(S_{INT})$ = 5m.

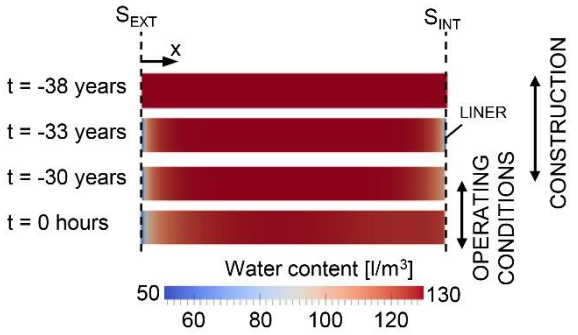

Figure 18 Evolution of the water content field though the thickness of the PCPV lateral wall during the first 38 years of life of the structure: construction (8 years) + normal operation (30 years).

The results of the mechanical analysis are presented in Figures 23, 24, 25 and 26 in terms of evolution of the tension in *Cable 8*. This is because *Cable 8* is the closest cable to the inner surface of the vessel and therefore the most affected by the fault.

The results obtained in the case of *short term* fault conditions analysis are reported in Figure 19 and Figure 20. Figure 19 shows that if no thermal strains are active, i.e. both steel and concrete are modelled as purely elastic materials - see curve (*a*) - the transient thermal has no effect of the stress state of the vessel. If the only FTS of the steel is activated - see curve (*b*) - a temporary loss in tension is obtained on heating. This is due to a thermal expansion of the steel tendon on heating, which causes a tensile stress relaxation, followed by a thermal contraction on cooling, allowing for a perfect recovery of the loss in tension developed on heating. By contrast, if only the PFTS of concrete is considered - see curve (*c*) – the tension in *Cable 8* increases on heating. This results from the thermal expansion of the concrete volume which causes the tendon to stretch on heating and

contract on cooling. Since steel FTS and concrete PFTS are of the same order of magnitude, the increase in tension associated to the steel FTS - curve (*b*) - is comparable to the absolute value of the loss in tension produced by the concrete PFTS - curve (*c*). This is the reason why if both steel FTS and concrete PFTS are activated the tension in *Cable 8* stays approximately steady during the whole heating-cooling cycle – see curve (*d*). If the moisture-independent part of LITS, that is PLITS, is also activated, curve (e) is obtained. This curve is obtained by using the full moisture dependent model presented in this paper and imposing dry conditions (i.e. a uniform field $\bar{C}$=0 l/m^3) to disregard the effects of drying. With this model, a drop in tension of about 8.5 % of the initial tension is obtained on heating which is not recovered on cooling. This is due to the irrecoverable development of contractive PLITS in the concrete, which causes a contraction of the steel tendon and thus a loss in pre-tension. If also the moisture-dependent thermal strain components are activated in the concrete model, curve (f) is obtained. This curve corresponds to full moisture dependent model used with the moisture field at the beginning of the accidental heating calculated through hygral analysis. That is, the expected moisture distribution after 30 years of normal operation of the vessel is considered. By using this model, a drop in tension of about 52.4 % of the initial tension is obtained. This is because all the moisture-dependent strains included in the constitutive model lead to a further contraction of the concrete volume. These results show that the moisture-dependent components of the concrete thermal strains play a key role in the stress redistribution taking place in a PCPV subjected to *short term* fault conditions. For the considered test case, the loss in tension in Cable 8 is significantly underestimated if the moisture dependency of the concrete thermal strain is not modelled; specifically, about 83 % of the loss in tension produced the accidental heating-cooling cycle is missed.

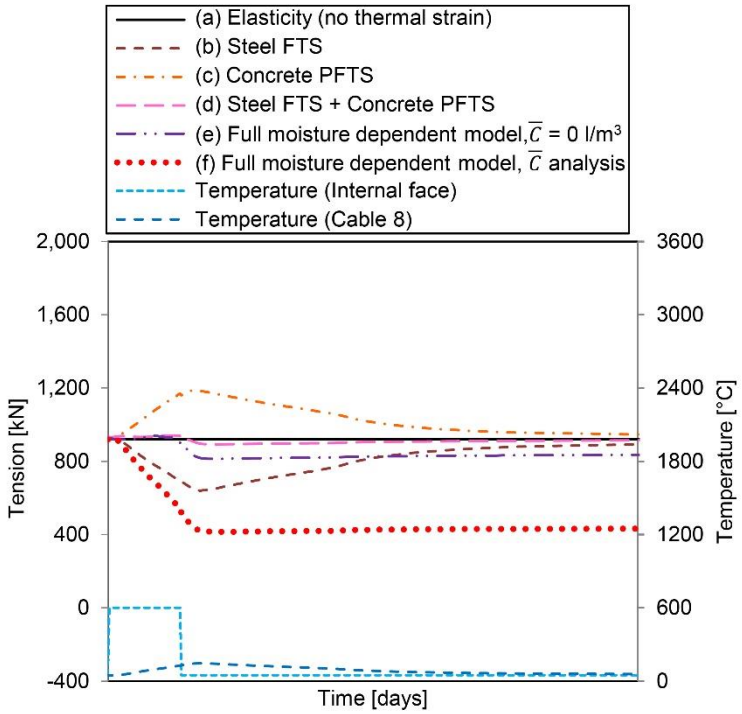

Figure 19 *Short term* fault condition (2 days): time evolution of the tension in Cable 8 obtained considering (a) Elasticity (no thermal strains), (b) only the Steel FTS, (c) only the Concrete PFTS, (d) Steel FTS + Concrete PFTS, (e) Steel FTS + Concrete PFTS + Concrete LITS, (f) Steel FTS + Full moisture-dependent concrete model. Evolution of the temperature at the inner surface of the vessel and at Cable 8.

Figure 20 shows the loss in tension obtained via the full moisture-dependent model and different initial moisture fields. It can be observed that a slightly larger drop in tension is obtained if a homogenous water content field of $\bar{C}$=130 l/m^3 is imposed - see curve (*h*) - than if the water field calculated through a thermo-hygral analysis is considered - see curve (*f*). However, due to the relatively high water content predicted via the thermo-hygral analysis in the region next to the inner surface of the vessel, the two curves are relatively close to each other. By contrast, if a homogenous water content field of $\bar{C}$=106 l/m^3 is imposed about 9.3 % of the tension drop is missed - see curve (*g*). These findings show that the behaviour of PCPV under fault conditions is highly sensitive to the moisture condition of the material at the beginning of the fault. Therefore, it is crucial to assess the actual hygral field prior to the mechanical analysis.

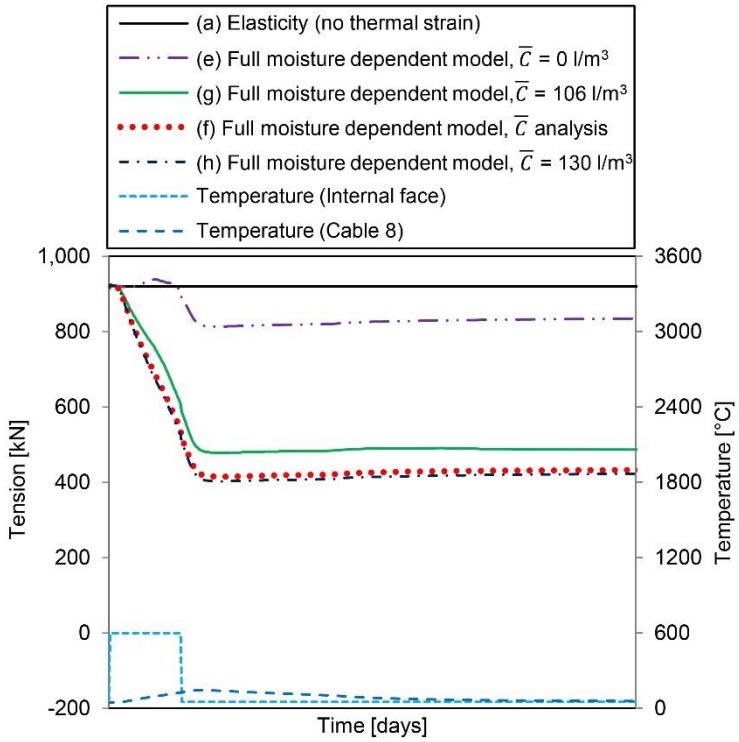

Figure 20 *Short term* fault condition (2 days): time evolution of the tension in Cable 8 obtained considering (a) Elasticity (no thermal strains), (e) Steel FTS + Concrete PFTS + Concrete LITS, (f) Steel FTS + Full moisture-dependent concrete model, (g) Steel FTS + Full moisture-dependent concrete model assuming $\bar{C}$=106 l/m^3, (h) Steel FTS + Full moisture-dependent concrete model assuming $\bar{C}$=130 l/m^3.

Similarly, the results obtained in the case of *long term* fault conditions have been reported in Figure 21 and Figure 22. If the full moisture-dependent model is adopted - see curve (*f*) in Figure 21 – a drop in tension of about 78 % of the initial pre-tension is obtained. In other words, a significantly larger tension loss is obtained for *long term* than for *short term* conditions. However, in the case of *long term* fault, only about 20 % of the tension loss is missed if the moisture-dependent strain components are disregarded – see curve (*g*) in Figure 21. This means that the portion of tension drop related to moisture-dependent strains is smaller for a *long term* fault than for a *short term* fault. This is because in the case of a *long term* fault the material next to the inner surface reaches considerably higher temperatures than in the case of a *short term* fault. Since the moisture-dependent thermal strains do not develop for temperatures higher than the drying temperature T_{dr} of 200 °C, their relative effect decreases progressively as the temperature rises above T_{dr}.

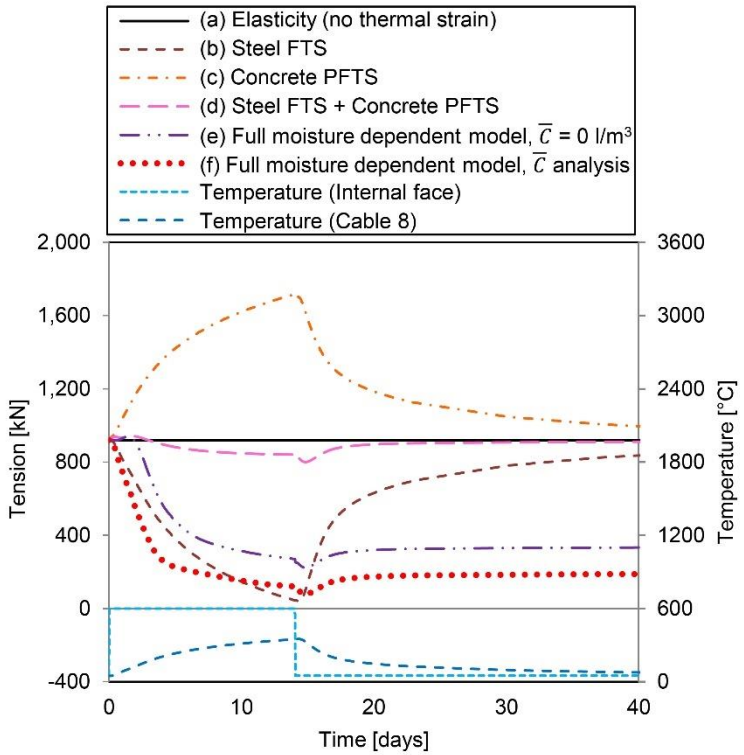

Figure 21 *Long term* fault condition (14 days): time evolution of the tension in Cable 8 obtained considering (a) Elasticity (no thermal strains), (b) only the Steel FTS, (c) only the Concrete PFTS, (d) Steel FTS + Concrete PFTS, (e) Steel FTS + Concrete PFTS + Concrete LITS, (f) Steel FTS + Full moisture-dependent concrete model. Evolution of the temperature at the inner surface of the vessel and at Cable 8.

As shown in Figure 22, if a homogeneous moisture content of $\bar{C}$=106 l/m^3 is considered - see curve (*g*) -, about 10.3 % of the tension drop is missed. This result shows that the assessment of the hygral field prior to the accidental-heating cooling fault is crucial also for PCPV subjected to long-term fault conditions.

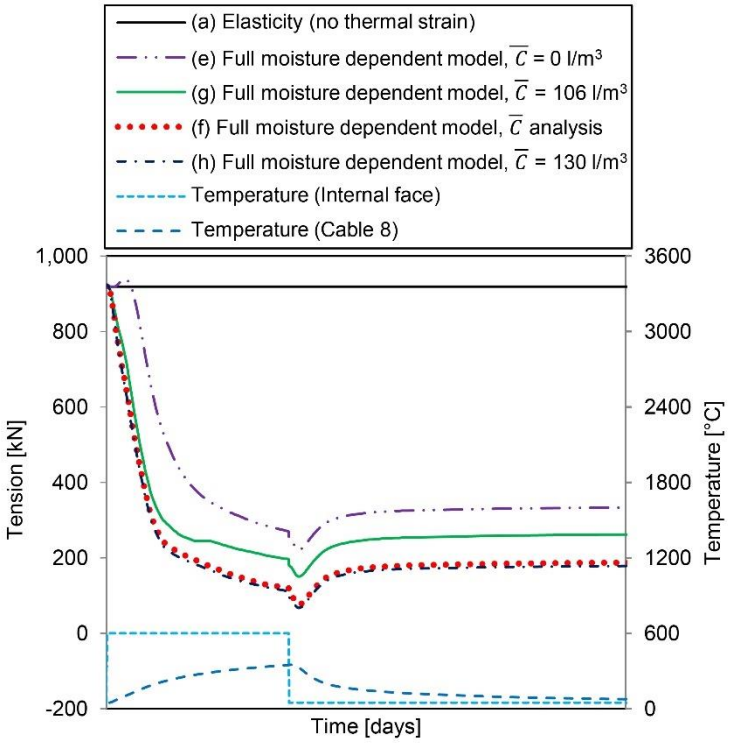

Figure 22 *Long term* fault condition (14 days): time evolution of the tension in Cable 8 obtained considering (a) Elasticity (no thermal strains), (e) Steel FTS + Concrete PFTS + Concrete LITS, (f) Steel FTS + Full moisture-dependent concrete model, (g) Steel FTS + Full moisture-dependent concrete model assuming $\bar{C}$=106 l/m^3, (h) Steel FTS + Full moisture-dependent concrete model assuming $\bar{C}$=130 l/m^3.

7 Conclusions

The following conclusions can be drawn from this study:

- A new strategy for modelling the dependency of high-temperature thermal strains on the moisture conditions of concrete prior to heating is presented.
- The approach explicitly models the moisture-dependent components of LITS and FTS. This allows the spatial variation of the material mechanical behaviour to be considered in structures with drying-induced moisture gradients.
- The proposed method allows the transient thermo-mechanical behaviour of the material as a function its moisture conditions at the beginning of thermal transient to be assessed. In other words, such an approach does not attempt to explicitly model the complicated and still not-well-understood moisture migration and evaporation phenomena occurring during high temperatures thermal transients. This allows modelling the thermo-hygro-mechanical problem through a simplified scheme involving a reasonably low number of parameters.

- The proposed moisture-dependent model allows assessing the effects of the age of a structure on its mechanical response under accidental conditions. By performing multiple analyses where accidental heating is assumed to occur at different times, the model can be used to perform design and predictive studies that account for the evolution of the thermo-mechanical performance of a structure with time. The model can also be used to perform forensic analyses. In this case, the moisture field at the beginning of heating can either be assessed numerically, as a function the age of the structure, or defined by the user if data on the moisture distribution are available.
- A limitation of this study is that it assumes the hygral boundary conditions of each material point to be comparable to those of the specimens studied in the experiments. Since the experiments considered in this work are performed on unsealed specimens, the model calibrated here might overestimate the contractive strain components due to concrete drying on heating. This means that the presented approach leads to a limit-solution based on the assumption of unobstructed water evacuation on heating. More experimental and numerical work needs to be done to investigate the effects of the hygral boundary conditions on the high temperature behaviour of the material.
- At the same time, the limitation discussed above represents a strength of the model. This is because the actual permeability and hygral boundary conditions of complex structures are often uncertain and fall between the two extreme conditions of obstructed and unobstructed water movement. This model can be adopted to assess these two limit-conditions by activating and deactivating the strain components related to the moisture movement on heating. Therefore, it represents a valuable tool for assessing the spectrum within which real material conditions fall.
- If new experiments became available, the approach could be adopted to model the behaviour of other concrete mixes.
- LITS plays a key role in the structural behaviour of bulk concrete structures subjected to accidental transient heating-cooling. In the case of nuclear PCPV, the loss in pretension caused by accidental heating-cooling cycles can be significantly underestimated if the moisture-dependent strain components are not explicitly modelled. Moreover, the assessment of the actual hygral field prior to heating is crucial to obtain realistic solutions.

8 Acknowledgements

This work was supported by EPSRC and EDF Energy.

References

[1] Torelli G, Mandal P, Gillie M, Tran V-X. Concrete strains under transient thermal conditions: A state-of-the-art review. Eng Struct 2016;127:172–88. doi:10.1016/j.engstruct.2016.08.021.

[2] Khoury GA, Grainger BN, Sullivan PJE. Transient thermal strain of concrete; literature review, conditions within specimen and behaviour of individual constituents. Mag Concr Res 1985;37:131–44.

[3] Schneider U, Kassel G. Properties of materials at high temperatures: Concrete. Gesamthochschul-Bibliothek; 1985.

[4] Holt M, Campbell RJ, Nikitin MB. Fukushima nuclear disaster. 2012.

[5] Abraham O, Dérobert X. Non-destructive testing of fired tunnel walls: The Mont-Blanc Tunnel case study. NDT E Int 2003;36:411–8. doi:10.1016/S0963-8695(03)00034-3.

[6] Yamashita H, Yoshida T, Hirashima T. Influence of water on load induced thermal strain of concrete. Proceeding 9th Int. Conf. Struct. Fire, 2016, p. 316–23.

[7] Khoury GA, Grainger BN, Sullivan PJE. Strain of concrete during first heating to 600 °C under load. Mag Concr Res 1985;37:195–215.

[8] Anderberg Y, Thelandersson S. Stress and deformation characteristics of concrete at high temperature: 2. Experimental investigation and material behaviour model. Bull. Div. Struct. Mech. Concr. Constr. Bull. 54, Lund: 1976, p. 86.

[9] Mindeguia J-C, Hager I, Pimienta P, Carré H, La Borderie C. Parametrical study of transient thermal strain of ordinary and high performance concrete. Cem Concr Res 2013;48:40–52.

[10] Kordina K, Ehm C, Schneider U. Effects Of Biaxial Loading On The High Temperature Behaviour Of Concrete. Fire Saf Sci 1986;1:281–90. doi:10.3801/IAFSS.FSS.1-281.

[11] Hansen CT, Eriksson L. Temperature Change Effect on Behavior of Cement Paste, Mortar, and Concrete Under Load. J Proc 1966;63. doi:10.14359/7635.

[12] Neville AM. Properties of concrete. 4th and final edition. 1995.

[13] Meyers SL. Thermal expansion characteristics of hardening cement paste and of concrete. Proc. Thirtieth Annu. Meet. Highw. Res. Board Held Washington, D.C., January 9-12, 1951, 1951, p. Vol 30, pp 193–203.

[14] Jeong J-H, Zollinger DG, Lim J-S, Park J-Y. Age and Moisture Effects on Thermal Expansion of Concrete Pavement Slabs. J Mater Civ Eng 2012;24. doi:10.1061/(ASCE)MT.1943-5533.0000342.

[15] Lim J-S, Moon K-H, Falchetto AC, Jeong J-H. Testing and modelling of hygro-thermal expansion properties of concrete. KSCE J Civ Eng 2016;20. doi:10.1007/s12205-015-0560-4.

[16] Pickett G. The Effect of Chang in Moisture-Content on the Crepe of Concrete Under a Sustained Load. ACI J Proc 1942;38.

[17] Torelli G, Gillie M, Mandal P, Tran V-X. A multiaxial load-induced thermal strain constitutive model for concrete. Int J Solids Struct 2016. doi:10.1016/j.ijsolstr.2016.11.017.

[18] De Soza T. Code_Aster: guide de lecture de la documentation de référence (http://www.code-aster.org) 2013.

[19] Helfer T, Michel B, Proix J-M, Salvo M, Sercombe J, Casella M. Introducing the open-source mfront code generator: Application to mechanical behaviours and material knowledge management within the PLEIADES fuel element modelling platform. Comput Math with Appl 2015;70:994–1023.

doi:10.1016/j.camwa.2015.06.027.

[20] Petkovski M, Crouch RS. Strains under transient hygro-thermal states in concrete loaded in multiaxial compression and heated to 250 °C. Cem Concr Res 2008;38:586–96.

[21] Illston JM, Sanders PD. Effect of temperature change upon the creep of mortar under torsional loading. Mag Concr Res 1973;25:136–44.

[22] Illston JM, Sanders PD. Chatacteristics and prediction of creep of a saturated mortar under variable temperature. Mag Concr Res 1974;26:169–79.

[23] Parrott LJ. Study of transitional thermal creep in hardened cement paste. Mag Concr Res 1979;31:99–103.

[24] Fahmi HM, Polivka M, Bresler B. Effects of sustained and cyclic elevated temperature on creep of concrete. Cem Concr Res 1972;2:591–606. doi:10.1016/0008-8846(72)90113-5.

[25] Colina H, Sercombe J. Transient thermal creep of concrete in service conditions at temperatures up to 300°C. Mag Concr Res 2004;56:559–74.

[26] Hassen S, Colina H. Transient thermal creep of concrete in accidental conditions at temperatures up to 400°C. Mag Concr Res 2006;58:201–8. doi:10.1680/macr.2006.58.4.201.

[27] Torelli G, Mandal P, Gillie M, Tran V-X. A confinement-dependent load-induced thermal strain constitutive model for concrete subjected to temperatures up to 500 °C. Int J Mech Sci 2018;144. doi:10.1016/j.ijmecsci.2017.12.054.

[28] Martin N. Experimental validation of the damage-plasticity modeling concept for normal strength concrete in fire. J Struct Fire Eng 2018;9:53–62. doi:10.1108/JSFE-01-2017-0001.

[29] Gernay T, Millard A, Franssen J-M. A multiaxial constitutive model for concrete in the fire situation: Theoretical formulation. Int J Solids Struct 2013;50:3659–73. doi:10.1016/j.ijsolstr.2013.07.013.

[30] Zienkiewicz OC. The finite element method. London: McGraw-hill; 1977.

[31] EDF. “Algorithme Non Linéaire Quasi-Statique STAT_NON_LINE.” Référence du Code Aster R5.03.01 révision : 10290. . (http://www.code-aster.org) 2013.

[32] Granger L. Comportement différé du béton dans les enceintes de centrales nucléaires. Analyse et modélisation. PhD Thesis. Ecole Nationale des Ponts et Chaussées, 1996.